



Supporting Information

for *Small*, DOI: 10.1002/smll.202100487

A Self-Ordered Nanostructured Transparent Electrode
of High Structural Quality and Corresponding Functional
Performance

*Dirk Döhler, Andrés Triana, Pascal Büttner, Florian
Scheler, Eric S.A. Goerlitzer, Johannes Harrer,
Anna Vasileva, Ezzeldin Metwalli, Wolfgang Gruber,
Tobias Unruh, Alina Manshina, Nicolas Vogel, Julien
Bachmann, and Ignacio Mínguez-Bacho**

Supporting Information

A self-ordered nanostructured transparent electrode of high structural quality and corresponding functional performance

Dirk Döhler,[†] Andrés Triana,[†] Pascal Büttner,[†] Florian Scheler,[†] Eric S.A. Goerlitzer,[‡] Johannes Harrer,[‡] Anna Vasileva,[¶] Ezzeldin Metwalli,[§] Wolfgang Gruber,[§] Tobias Unruh,[§] Alina Manshina,[¶] Nicolas Vogel,[‡] Julien Bachmann,^{†,¶} and Ignacio Mínguez-Bacho^{*,†}

[†]*Chemistry of Thin Film Materials, Department of Chemistry and Pharmacy, Friedrich-Alexander University Erlangen-Nürnberg, Cauerstr. 3, Erlangen, 91058 Germany*

[‡]*Institute of Particle Technology, Friedrich-Alexander University Erlangen-Nürnberg, Cauerstraße 4, 91058 Erlangen, Germany*

[¶]*Institute of Chemistry, Saint-Petersburg State University, Universitetskii pr. 26, St. Petersburg, 198504 Russia*

[§]*Institute for Crystallography and Structure Physics, Friedrich-Alexander University Erlangen-Nürnberg, Staudtstr. 3, Erlangen, 91058 Germany*

E-mail: ignacio.minguez@fau.de

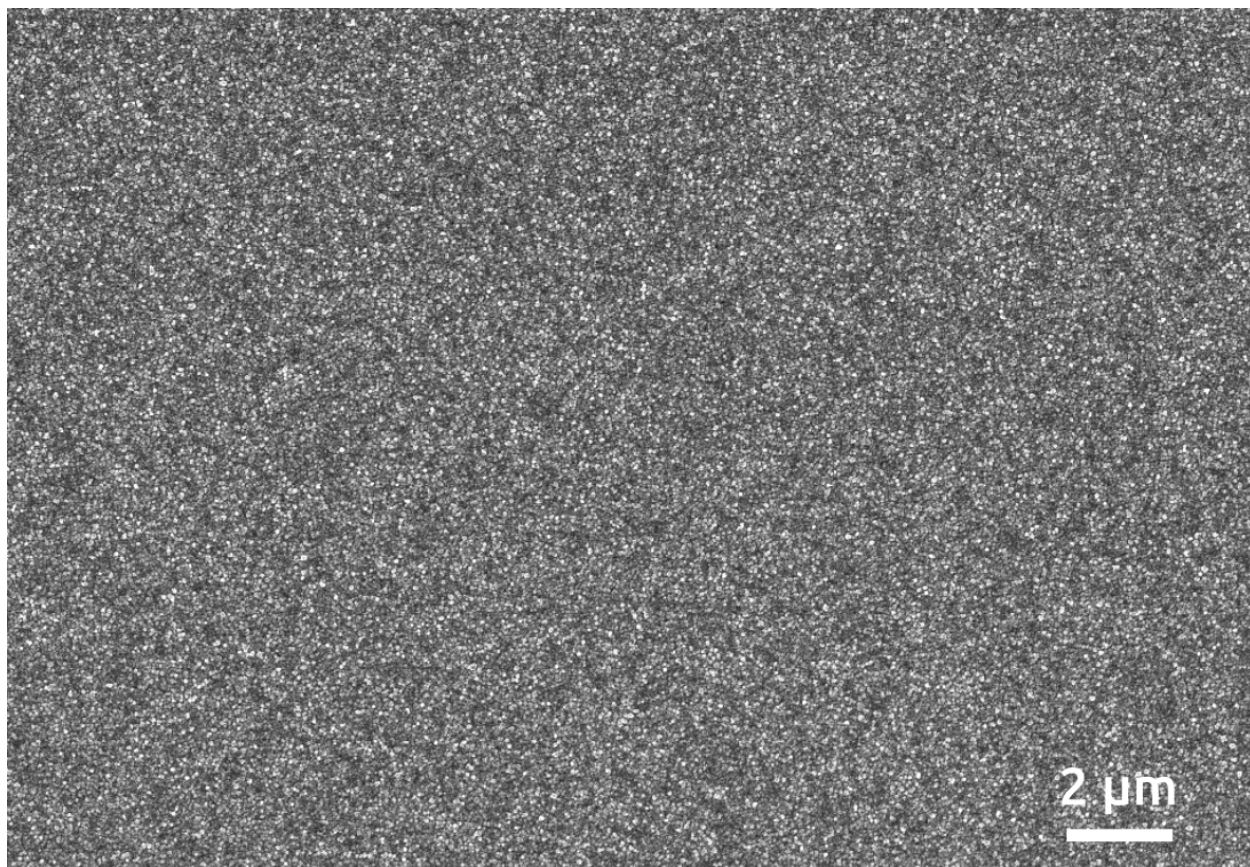


Figure S1: Top view SEM micrograph of an evaporated Al film on a glass / ITO / TiO₂ substrate.

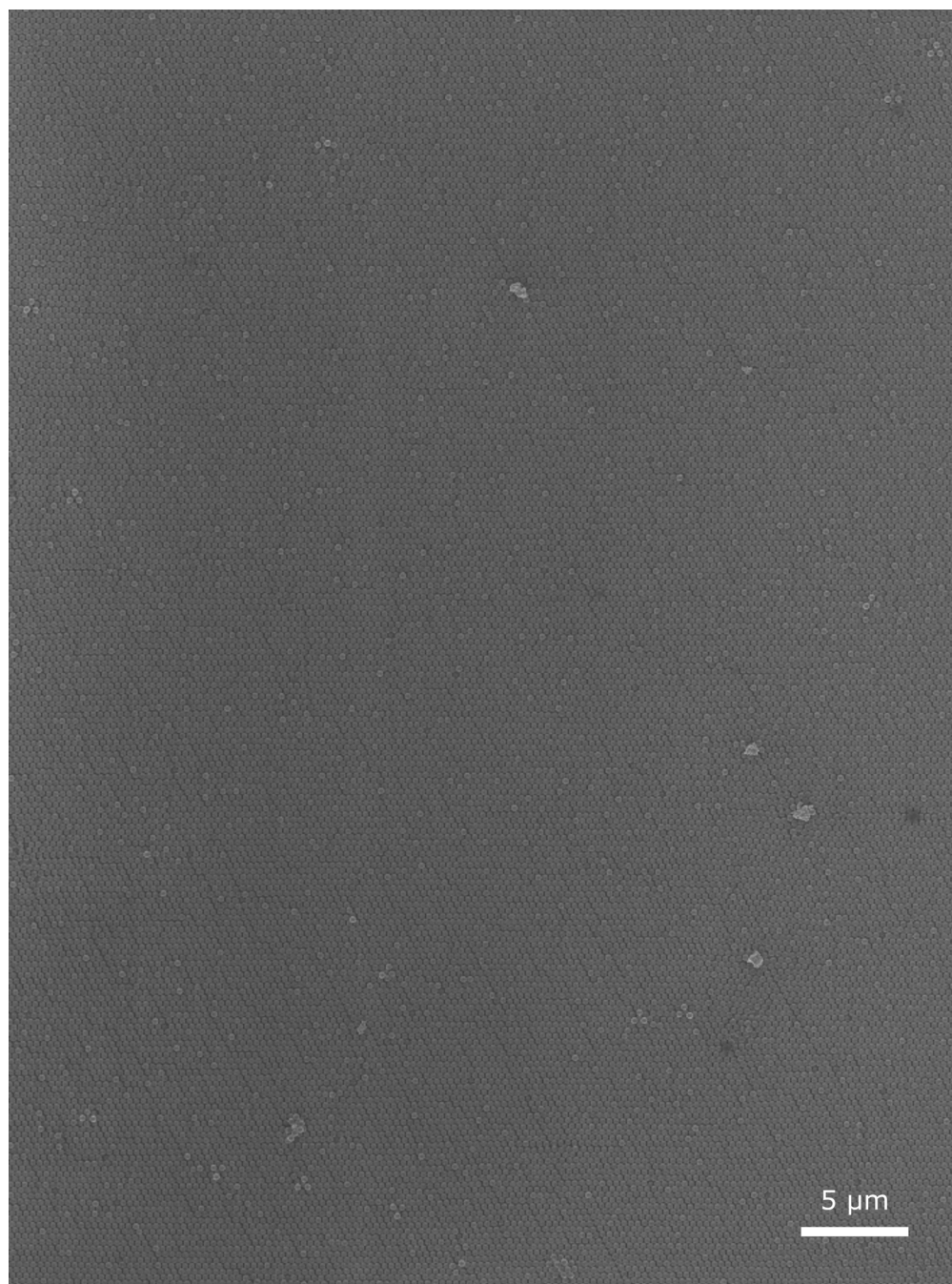


Figure S2: Top view SEM micrograph of a single domain PS spheres array over an area of $60 \times 41 \mu\text{m}$.

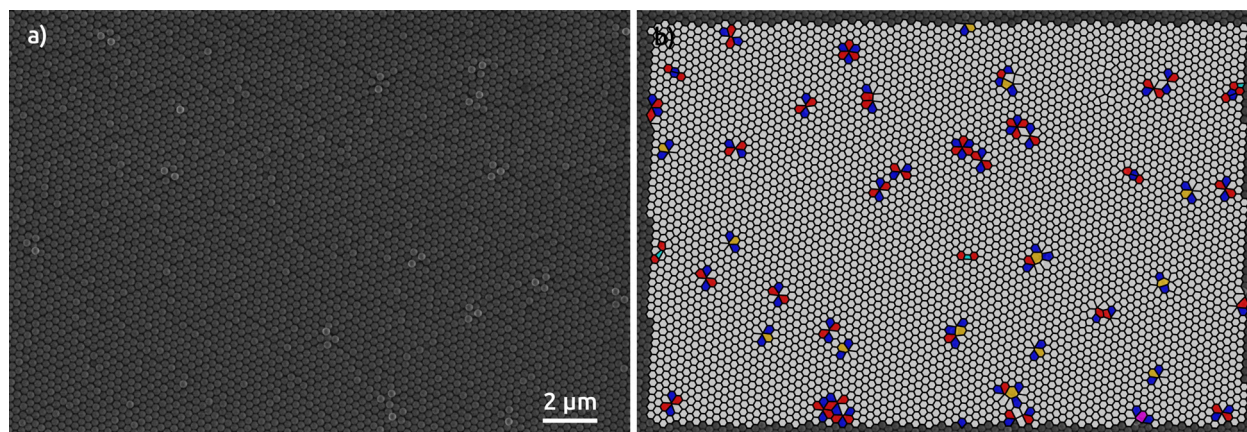


Figure S3: a) Top view SEM micrograph and b) the corresponding analysis of the defect detection on the arrangement of PS spheres. The colours indicate the number of first neighbours as follows: blue - 5 neighbours, white - 6 neighbours, red - 7 neighbours and yellow - 8 neighbours. The sample image contains a 3.9% of defects from a total 4943 spheres analysed.

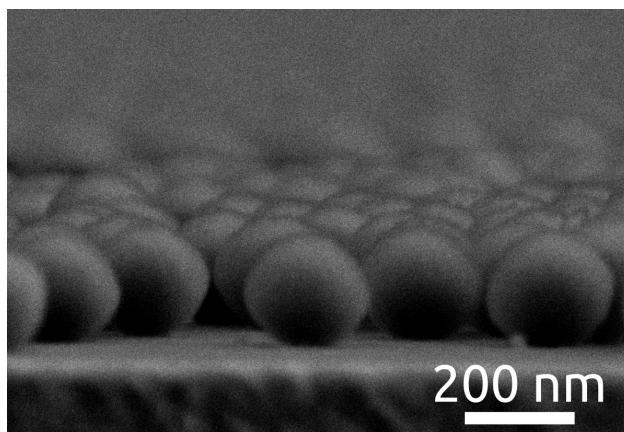


Figure S4: SEM micrograph of PS spheres after etching under oxygen plasma at 50 W for 9 minutes keeping the chamber pressure at 0.2 mbar and an oxygen flow rate of 5 sccm.

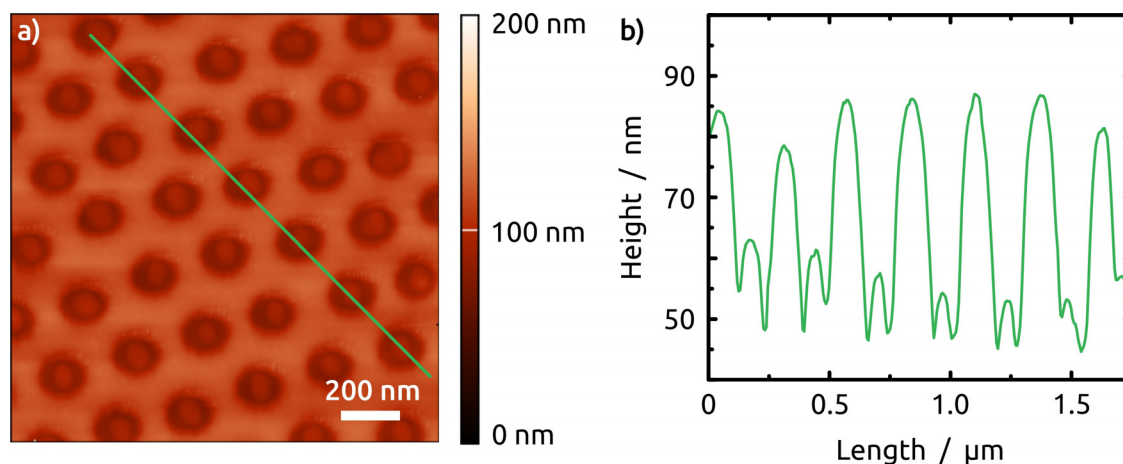


Figure S5: a) AFM micrograph of a SiO₂ pattern left after removing PS sphere array on a Si/SiO₂ wafer; b) profile of the green line on the AFM micrograph showing a SiO₂ thickness of 40 nm and a periodicity of 280 nm. The bumps observed in the centers of the holes are polymer residues left after detaching the PS spheres at each contact point. [M.J. Skaug, B.M. Coffey and D.K. Schwartz *ACS Applied Materials and Interfaces*, **2013**, *5*, 12854-12859].

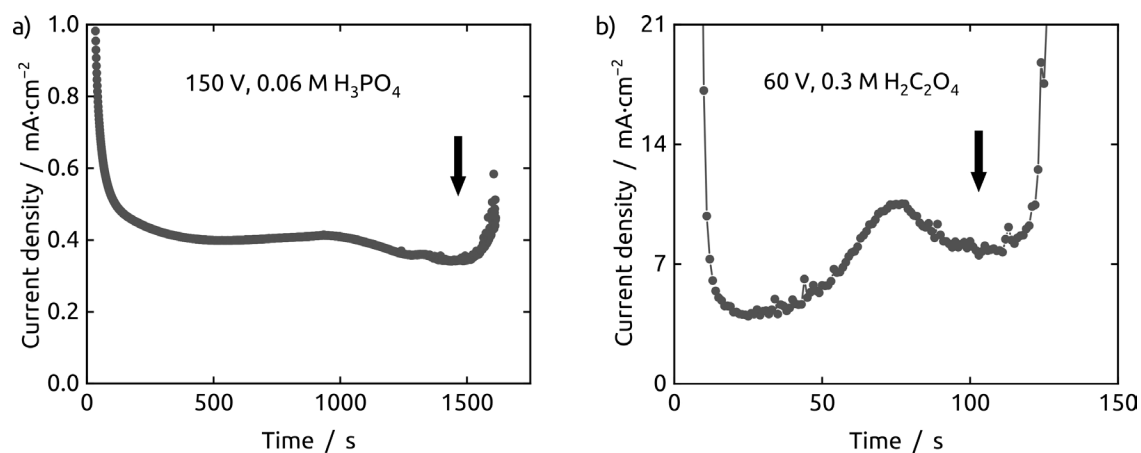


Figure S6: Chronoamperometric curves of anodization processes at a) 150 V, 0.06 M H₃PO₄, and b) 60 V, 0.3 M H₂C₂O₄ aqueous electrolytes. The arrow points the moment where the anodization must be stopped. Continuing further results in oxygen bubble evolution and eventual delamination of the alumina layer.

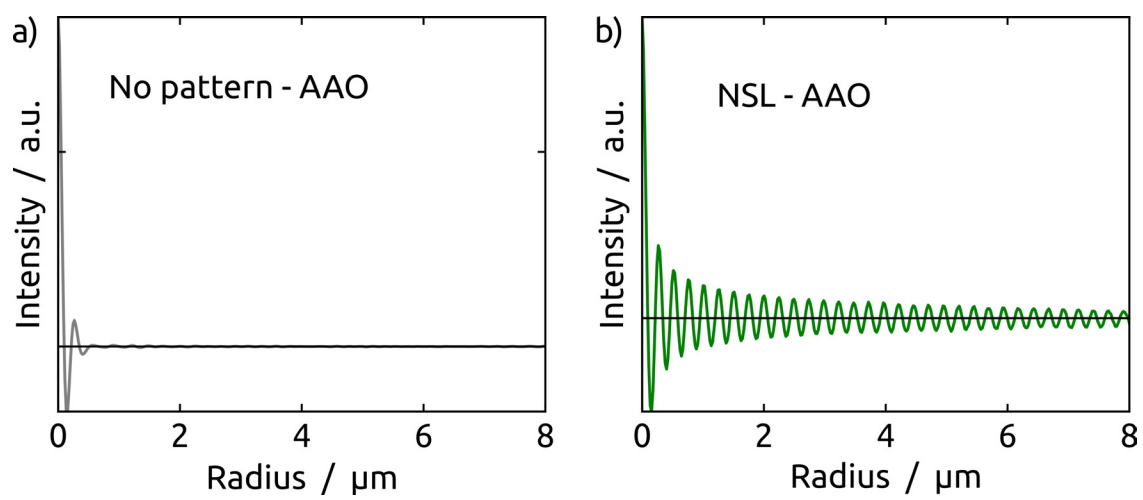


Figure S7: Radial average obtained from the SCI images from a) disordered and b) hexagonally ordered nanopores.



Figure S8: Top view SEM micrograph of a nanoporous single domain array over an area of $60 \times 41 \mu\text{m}$.

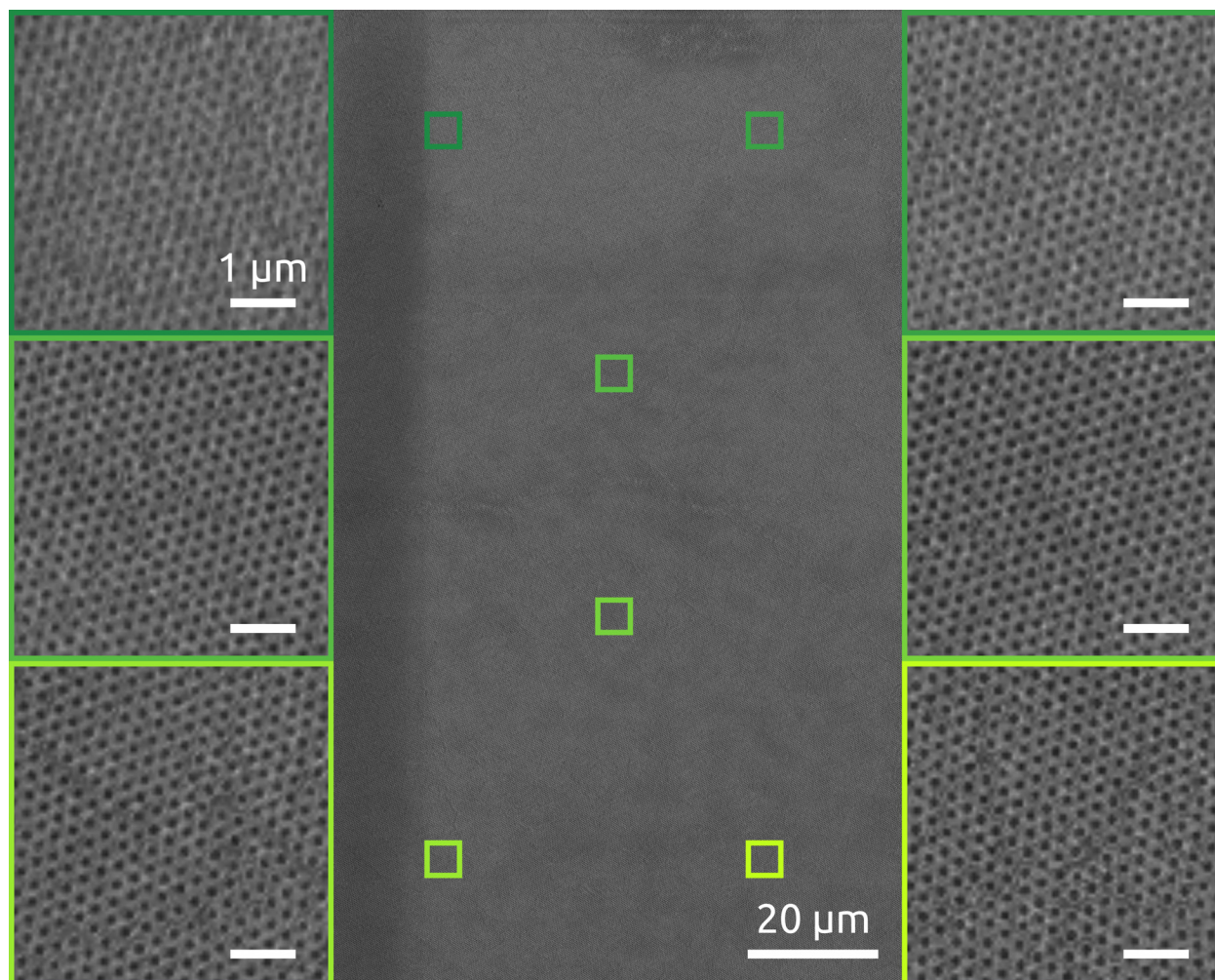


Figure S9: Top view SEM micrograph of a nanoporous single domain array over an area of $85 \times 150 \mu\text{m}$. Since the low magnification does not allow one to identify individual pores, the insets taken at various locations of the same micrograph demonstrate that they all belong to the same domain given the pore alignment.

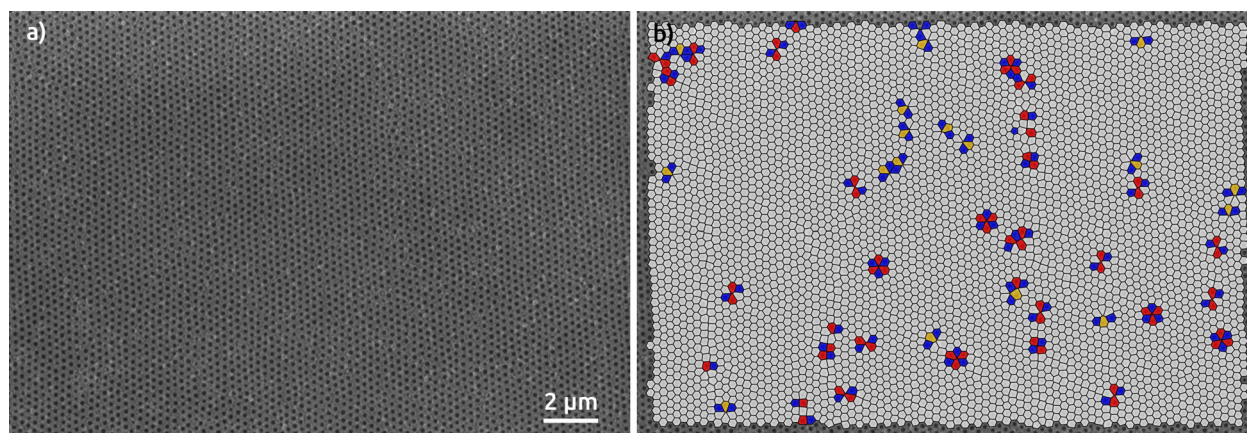


Figure S10: a) Top view SEM micrograph and b) the corresponding analysis of the defect detection on the arrangement of nanoporous AAO. The colours indicate the number of first neighbours as follows: blue - 5 neighbours, white - 6 neighbours, red - 7 neighbours and yellow - 8 neighbours. The sample image contains a 4.2% of defects from a total 4972 nanopores analysed.

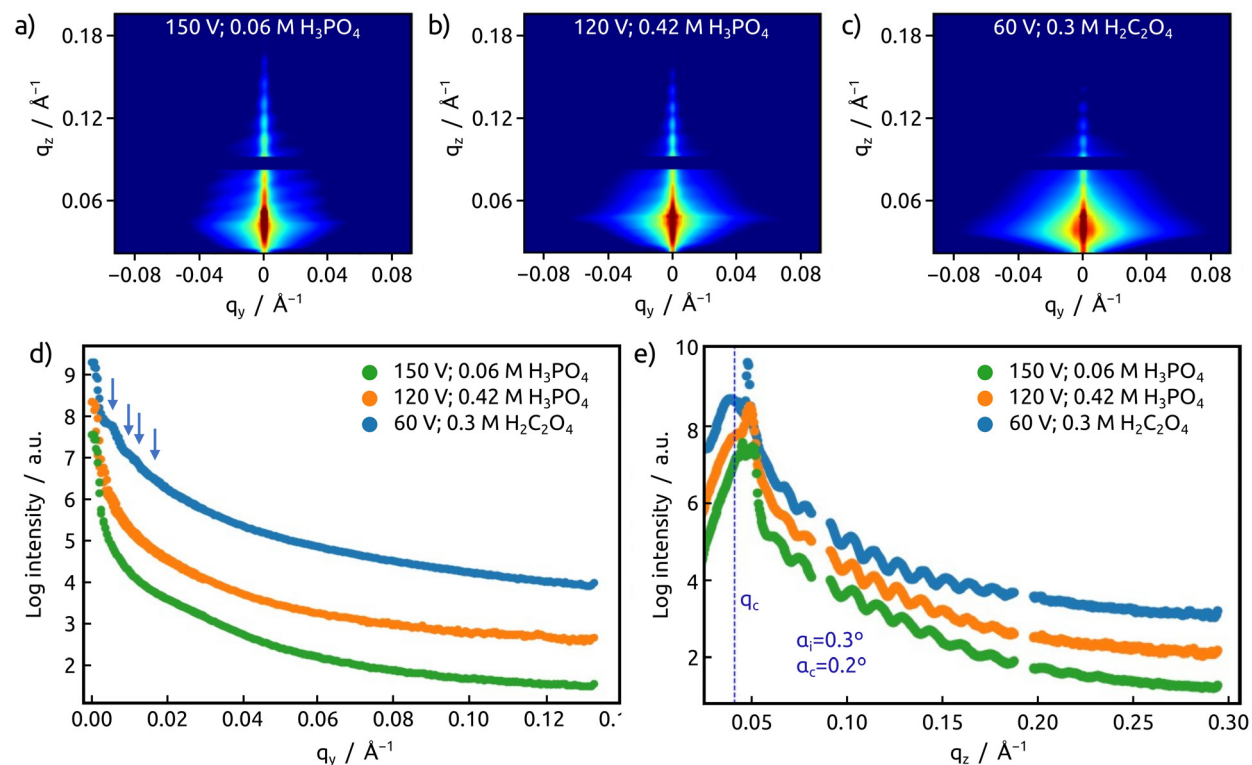


Figure S11: 2D GISAXS patterns recorded at an incident angle of 0.3° , for pre-patterned samples anodized under the following experimental conditions: a) 150V (0.06 M H_3PO_4), b) 120V (0.42 M H_3PO_4) and c) 60V (0.3 M $\text{H}_2\text{C}_2\text{O}_4$); GISAXS d) q_y profiles and (e) GISAXS q_z profiles of nanoporous AAO layers grown on NSL pre-patterned glass/ ITO / TiO_2 / Al substrates after wet chemical etching. Pores with periodic distance of 280 nm cannot be detected at a maximum sample-to-detector distance (1.598 m) of the employed system. From the main characteristic q_y peak a domain spacing was calculated to be 130 nm and four peaks were observed at scattering vector ratios with square roots of 1:3:4:7 relative to the first-order peak indicating a hexagonally ordered structure. From a critical scattering vector (q_c) indicate a top SiO_2 layer that persists during the whole the anodization process (dotted line).

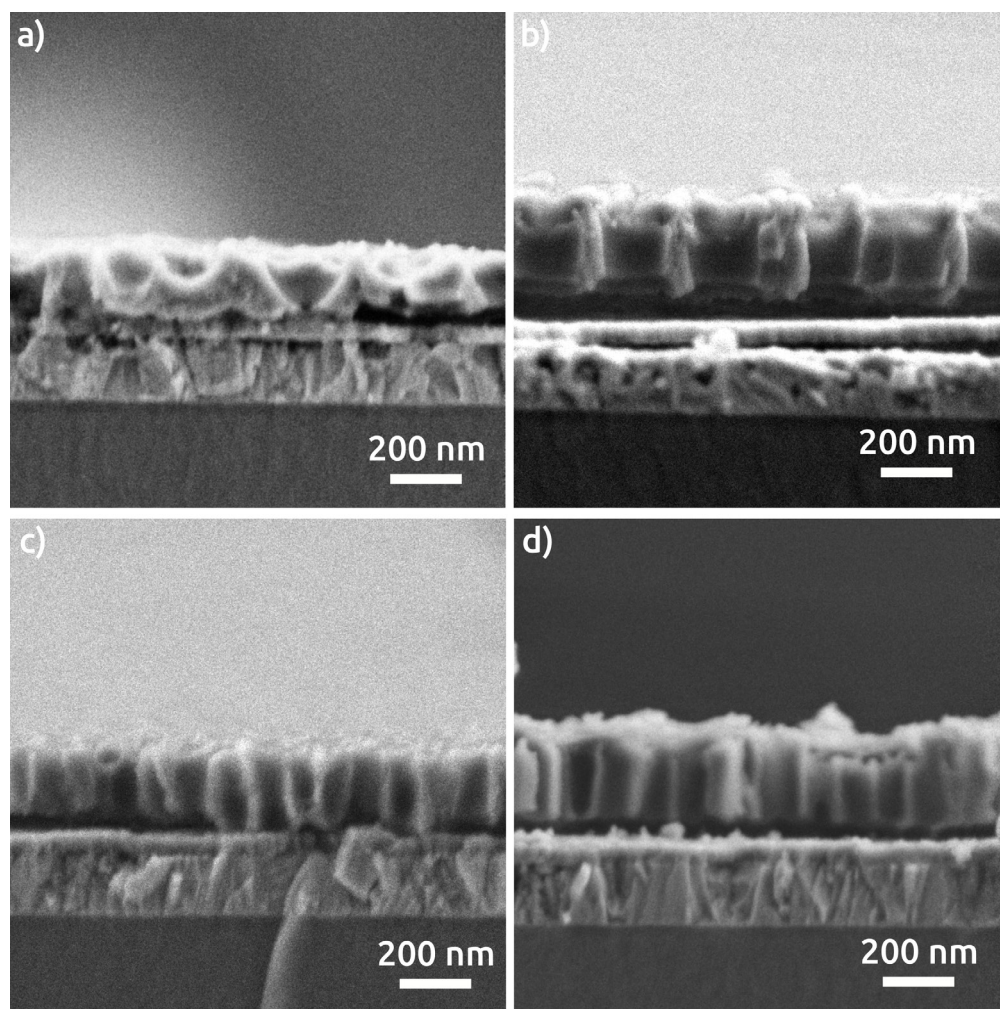


Figure S12: Cross section SEM micrographs of AAO anodized in a) 150 V, 0.06 M H_3PO_4 without NSL pre-patterning and b) with NSL pre-patterning, c) 60 V, 0.3 M $\text{H}_2\text{C}_2\text{O}_4$ without NSL pre-patterning and d) with NSL pre-patterning. The images were taken after the specified chemical etching for each type of AAO as described in the experimental section.

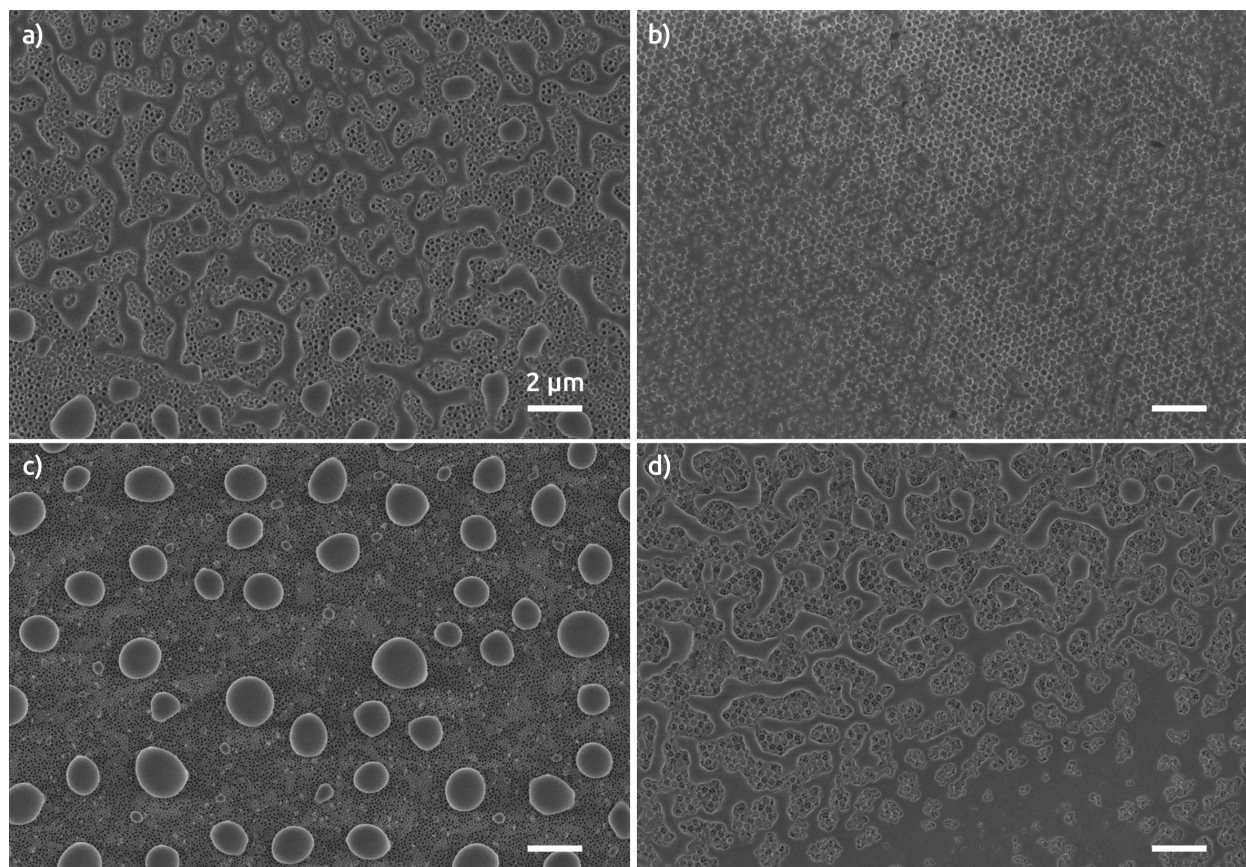


Figure S13: Top view SEM micrographs of dewetted Sb_2S_3 layers on AAO anodized in a) 150 V, 0.06 M H_3PO_4 without NSL pre-patterning and b) with NSL pre-patterning, c) 60 V, 0.3 M $\text{H}_2\text{C}_2\text{O}_4$ without NSL pre-patterning and d) with NSL pre-patterning.

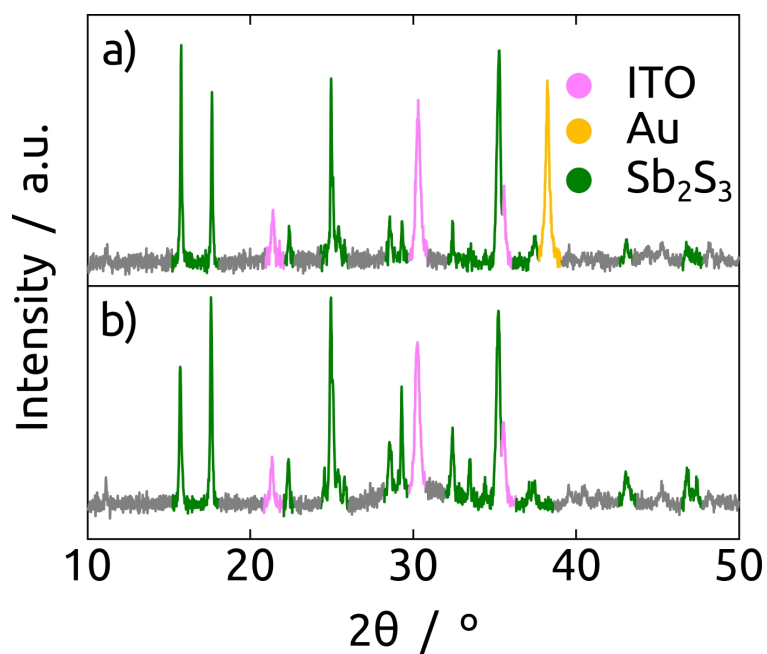


Figure S14: X-ray diffractograms of solar cells after redissolving the organic semiconductors; a) Substrate anodized in 150 V, 0.06 M H₃PO₄ with NSL pre-patterning and b) substrate anodized in 60 V, 0.3 M H₂C₂O₄ with NSL pre-patterning.

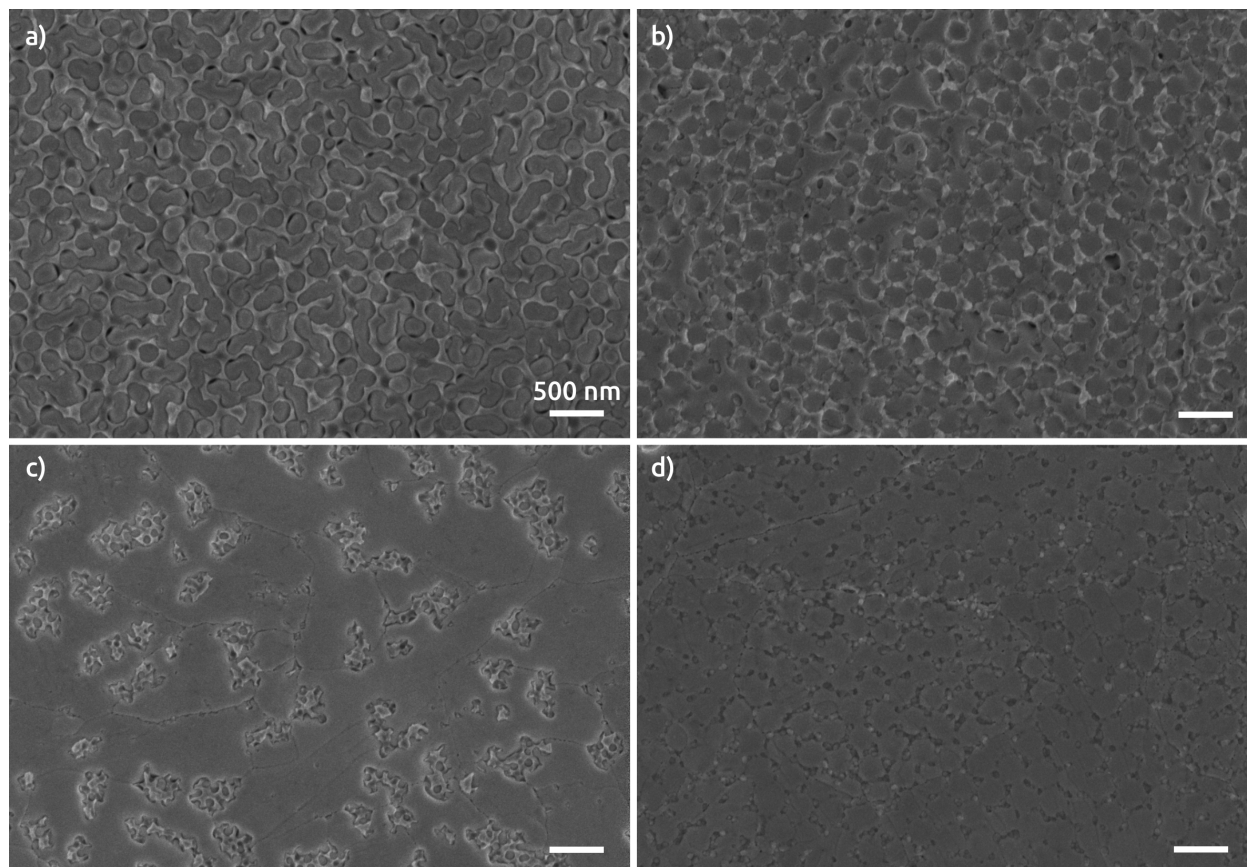


Figure S15: Top view SEM micrographs of Sb_2S_3 films with an underlying ZnS layer on AAO anodized in a) 150 V, 0.06 M H_3PO_4 without NSL pre-patterning and b) with NSL pre-patterning, c) 60 V, 0.3 M $\text{H}_2\text{C}_2\text{O}_4$ without NSL pre-patterning and d) with NSL pre-patterning.

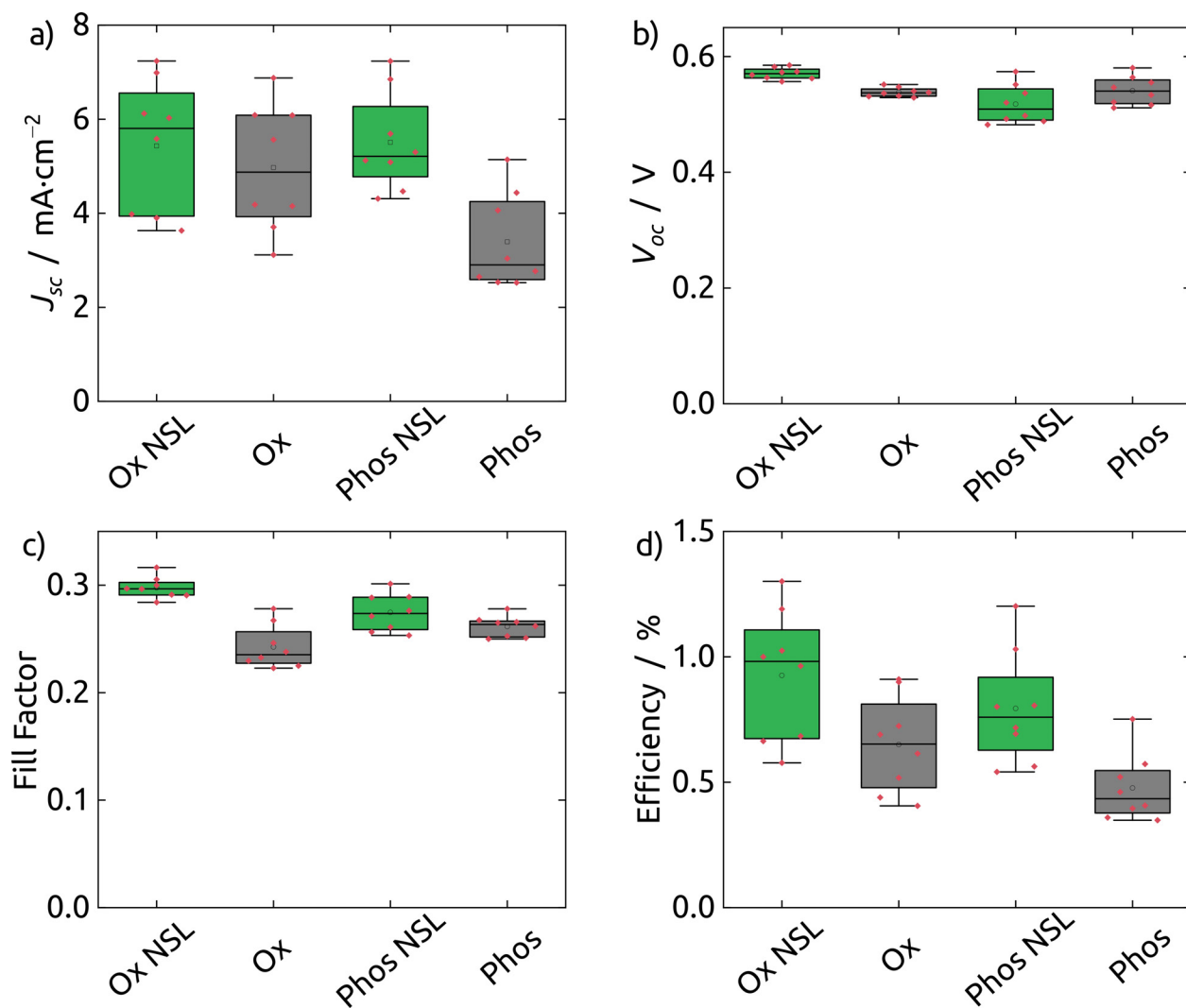


Figure S16: Solar cell statistics depending on the geometry of the electrodes; a) Short circuit current; b) Open circuit Voltage; c) Fill factor; d) Efficiency.

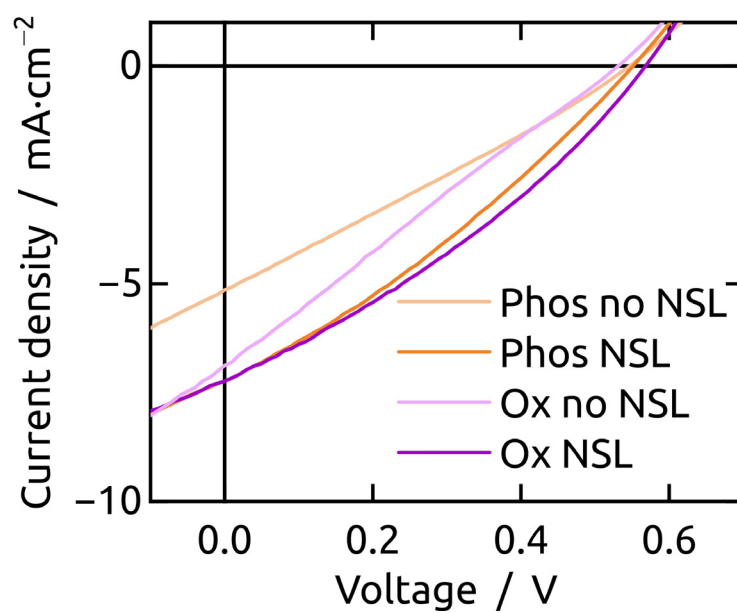


Figure S17: J - V curves of the champion cells built on electrodes anodized in 150 V, 0.06 M H_3PO_4 (purple) and 60 V, 0.3 M $\text{H}_2\text{C}_2\text{O}_4$ (orange) without (lighter colors) and with (darker colors) NSL pre-patterning.